

1 **Variation in CO₂ and CH₄ Fluxes Among Land Cover Types in Heterogeneous Arctic Tundra**
2 **in Northeastern Siberia**

3
4 Sari Juutinen^{1,2}, Mika Aurela¹, Juha-Pekka Tuovinen¹, Viktor Ivakhov³, Maiju Linkosalmi¹, Aleksii
5 Räsänen^{4,5}, Tarmo Virtanen⁴, Juha Mikola^{4,6}, Johanna Nyman¹, Emmi Vähä¹, Marina Loskutova⁷,
6 Alexander Makshtas⁷, and Tuomas Laurila¹

7
8 1) Finnish Meteorological Institute, Climate System Research, Erik Palménin aukio 1, 00560
9 Helsinki, Finland

10 2) Department of Geographical and Historical Studies, University of Eastern Finland,
11 Yliopistokatu 2, FI-80100 Joensuu, Finland (P.O. Box 111, FI-80101 Joensuu, Finland)

12 3) Voeikov Main Geophysical Observatory, Ulitsa Karbysheva, 7, St Petersburg, 194021,
13 Russia

14 4) Ecosystems and Environment Research Programme, University of Helsinki, Viikinkaari 1,
15 00790 Helsinki, Finland

16 5) Natural Resources Institute Finland (Luke), Paavo Havaksen tie 3,
17 90570 Oulu, Finland

18 6) Natural Resources Institute Finland (Luke), Latokartanonkaari 9,
19 00790 Helsinki, Finland

20 7) Arctic and Antarctic Research Institute, Bering str., 38, St Petersburg, 199397, Russia

21
22
23 Corresponding author Sari Juutinen, sari.juutinen@uef.fi
24
25
26

Formatted: Top: 2 cm, Bottom: 2 cm

27 **Abstract**

28 Arctic tundra is facing unprecedented warming, resulting in shifts in the vegetation, thaw regimes,
29 and potentially in the ecosystem-atmosphere exchange of carbon (C). However, the estimates of
30 regional carbon dioxide (CO₂) and methane (CH₄) budgets are highly uncertain. We measured CO₂
31 and CH₄ fluxes, vegetation composition and leaf area index (LAI), thaw depth, and soil wetness in
32 Tiksi (71° N, 128° E), a heterogeneous site located within the prostrate dwarf-shrub tundra zone in
33 northeastern Siberia. Using the closed chamber method, we determined the net ecosystem exchange
34 (NEE) of CO₂, ~~dark~~-ecosystem respiration (~~ER~~) in the dark (ER), ecosystem gross photosynthesis
35 (Pg), and CH₄ fluxes during the growing season. We applied a previously developed high-spatial-
36 resolution land-cover map over an area of 35.8 km² for spatial extrapolation. Among the land-
37 cover types varying from barren to dwarf-shrub tundra and tundra wetlands, the NEE and Pg at the
38 photosynthetically active photon flux density of 800 μmol m⁻² h⁻¹ (NEE₈₀₀ and Pg₈₀₀) were greatest
39 in the graminoid-dominated habitats, i.e., streamside meadow and fens, with NEE₈₀₀ and Pg₈₀₀ of
40 up to -21 (uptake) and 28 mmol m⁻² h⁻¹, respectively. Vascular LAI was a robust predictor of both
41 NEE₈₀₀ and Pg₈₀₀ and, on a landscape scale, the fens were disproportionately important for the
42 summertime CO₂ sequestration. Dry tundra, including the dwarf-shrub ~~dominated vegetation~~ tundra
43 and lichen tundra ~~and barren~~, had smaller CO₂ exchange rates. The fens were the largest the
44 dominant source of CH₄, while the dry mineral soil tundra consumed atmospheric CH₄, which on a
45 landscape scale amounted to -9 % of the total CH₄ balance during the growing season. The largest
46 seasonal mean CH₄ consumption rate of 0.02 mmol m⁻² h⁻¹ occurred in sand- and stone-covered
47 barren. The high consumption rate agrees with the estimate based on the eddy covariance
48 measurements at the same site. We acknowledge the uncertainty involved in spatial extrapolations
49 due to a small number of replicates per land-cover type. This study highlights the need to
50 distinguish different land-cover types including the dry tundra habitats to account for their different
51 CO₂ and CH₄ flux patterns, especially the consumption of atmospheric CH₄, when estimating tundra
52 C exchange on a larger spatial scale.

53

54 **1 Introduction**

55 It is uncertain whether the Arctic tundra is a sink or a source of atmospheric carbon (C). The current
56 estimates suggest a sink of 13–110 Tg C yr⁻¹, but their uncertainty range crosses the zero balance
57 (McGuire et al. 2012, Virkkala et al. 2020). Improving these estimates is vital, because the Arctic
58 tundra covers a vast area of 7.6 million km² (Walker 2000) that is experiencing substantial warming
59 (IPCC 2013, Chen et al. 2021). Warming can alter C exchange, ~~and~~ either amplifying or mitigating
60 climate change through ecosystem–atmosphere interactions. Some local-scale studies suggest that
61 the Arctic tundra is shifting from a small sink to a source of C (Webb et al. 2016, Euskirchen et al.
62 2017). It is likely that the climate change response of the ecosystem carbon dioxide (CO₂) sink
63 strength and methane (CH₄) emissions, whether an increase or a decrease, depends on site-specific
64 changes in thawing, wetness, temperature, and vegetation (McGuire et al. 2018). Dynamics of C
65 exchange needs to be quantified across the ~~Arctic~~ ~~arctic~~ habitats to improve the upscaling of arctic
66 CO₂ and CH₄ balances and to monitor how ecosystems respond to environmental changes.

67 The uncertainty in the arctic C balance estimates arises from the sparse and uneven
68 observation network, which provides poor support for model-based spatial extrapolation (cf.
69 McGuire et al. 2018, Virkkala et al. 2021, Kuhn et al. 2021). On a local scale, landscape
70 heterogeneity and the related difficulty of mapping the spatial distribution of habitats and their C
71 fluxes add to this uncertainty (McGuire et al. 2012, Treat et al. 2018, Saunois et al. 2020). ~~In~~
72 ~~addition~~ Furthermore, year-to-year variations in seasonal features, particularly the timing of spring,
73 summer temperatures, and snow depth have been found to cause substantial variation in the annual
74 ~~net~~ CO₂ and CH₄ balances (Aurela et al. 2004, Humphreys and Lafleur 2011, Zhang et al. 2019).
75 Fine-scale spatial heterogeneity in soil water saturation, thaw depth, vegetation characteristics, and
76 soil organic content is typical of the tundra landscape (e.g., Virtanen and Ek 2014, Mikola et al.
77 2018, Lara et al. 2020). These factors control CO₂ and CH₄ exchange, and on an annual scale,
78 tundra wetlands typically act as net CO₂ sinks while upland tundra areas have a close-to-neutral

79 CO₂ balance (e.g., Marushchak et al. 2013, Virkkala et al. 2021). While tundra wetlands are
80 substantial sources of CH₄, dry tundra acts as a small sink or small source of atmospheric CH₄
81 (Bartlett and Harriss 1993, Kuhn et al. 2021).

82 Mineral soil tundra barrens, however, have been found to have high consumption rates
83 of atmospheric CH₄, which is due to the high-affinity methane oxidizing bacteria (Emmerton et al.
84 2014, Jørgensen et al. 2014, D'Imperio et al. 2017, Oh et al. 2020). These bacteria can utilize
85 atmospheric CH₄ as energy source at low atmospheric concentrations, opposite to the low-affinity
86 methane oxidizers that require higher CH₄ concentrations and occur in wetlands (e.g., Oh et al.
87 2020). A modeling exercise that introduced the high-affinity methanotrophy for mineral-rich soils
88 resulted in a doubling of the circumpolar soil CH₄ sink above 50° N compared to previous estimates
89 (Oh et al. 2020). Thus, distinguishing dry and wet tundra with their moisture and vegetation
90 characteristics is crucial when mapping C exchange within the tundra biome. Treat et al. (2018)
91 tested spatial resolution requirements for such mapping on a landscape level and found that a 20-m
92 pixel size captured the spatial variation in a reasonable manner, while a coarser resolution resulted
93 in underestimation of both the landscape-scale CO₂ uptake and CH₄ emissions. In addition,
94 understanding the spatial heterogeneity of ecosystem C exchange substantially improves analyses of
95 eddy covariance (EC) measurements that, while in principle representing spatially integrated fluxes,
96 may provide biased gas flux balances in a highly heterogeneous source/sink environment, as the
97 spatial integration of EC involves non-uniform weighting of the surface elements that contribute to
98 the measured flux (Tuovinen et al. 2019).

99 The aim of this study was to assess the spatial patterns and magnitudes of CO₂ and
100 CH₄ fluxes within heterogeneous prostrate dwarf-shrub tundra in Tiksi, located in northeastern
101 Russia. Growing season fluxes of CO₂ (ecosystem net exchange, photosynthesis, and respiration)
102 and CH₄ were determined using the chamber method to answer the questions: (i) what is the
103 magnitude of these fluxes in different land-cover types and (ii) how do they depend on vegetation

104 characteristics and soil wetness? In addition, we extrapolated the plot-level measurements in space
105 and compared them with the ecosystem-level data measured with the EC technique.

106

107 **2 Materials and Methods**

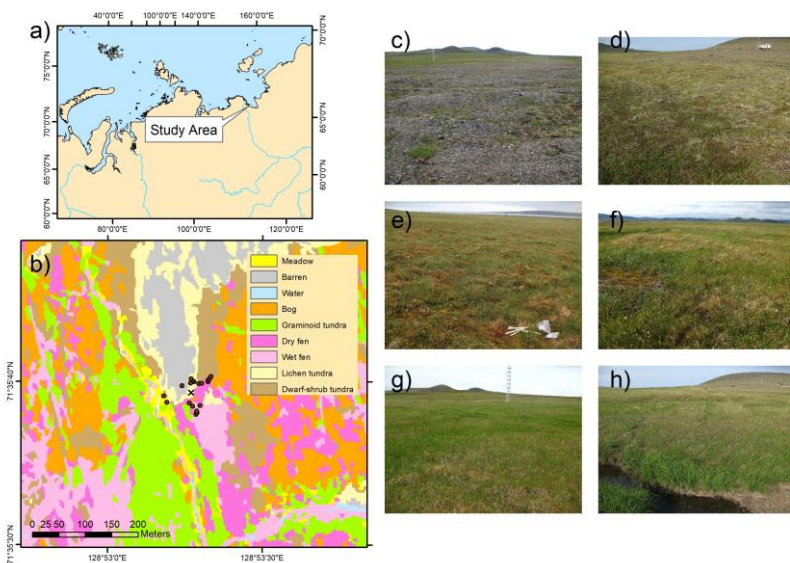
108 *2.1 Study site*

109 The study site is located near the Tiksi Observatory in Sakha (Yakutia) (see Uttal et al. 2016),
110 northeastern Russia (71.5943° N, 128.8878° E), 500 m inland off the Laptev Sea coast and, on
111 average, 7 m above sea level (Fig. 1a). The area belongs to the middle-arctic prostrate dwarf-shrub
112 tundra subzone (Walker, 2000) and has continuous permafrost. In the end of the growing season,
113 the maximum thaw depth is *ca.* 40 cm (Mikola et al. 2018). The climate in Tiksi is defined by cold
114 winters and cool summers. The long-term mean annual temperature and mean annual precipitation
115 were -12.7 °C and 232 mm, respectively, during the climate normal period 1981–2010. [The](#)
116 [growing season lasts about 3 months, and the soils typically freeze in the end of September, and the](#)
117 [permanent snow falls in October and thaws in June \(AARI 2018\).](#)

118 Bedrock is alkaline, resulting in high plant species richness. Vegetation consists of
119 mosses, lichens, grasses, sedges, prostrate dwarf-shrubs such as willows (*Salix* spp.), dwarf birch
120 (*Betula nana*), and *Diapensia lapponica*, and forb species (Table 1). The average heights of dwarf-
121 shrub species are 4–6 cm, and the leaf area index (LAI) of vascular plants reaches up to 1 m² m⁻² in
122 the fen and meadow habitats with graminoid vegetation (Juutinen et al. 2017). The land cover at the
123 site has been classified a priori and mapped based on a combination of field inventories and high-
124 spatial-resolution satellite images (Mikola et al. 2018). The a priori land-cover types (LCTs)
125 consist of wet fen, dry fen, graminoid tundra, bog, meadow at the stream bank, dwarf-shrub tundra,
126 and lichen tundra that consists of barren ground with rocks and sand and patches of vegetation
127 (Table 1, Fig. 1 c–h; for a closer view see Fig. A1). [The depth of the organic layer depth is](#)
128 [negligible in lichen tundra and a few centimeters in dwarf-shrub tundra, meadow, and graminoid](#)
129 [tundra. In bog, dry fen, and wet fen, the organic layer depth is at least the maximum depth of the](#)

130 active layer, *ca.* 30–40 cm. Soil organic content [can](#) reach *ca.* 40 % in tundra wetlands (Mikola et
 131 al. 2018). A section of the wet and dry fen within the EC footprint area is disturbed by vehicle
 132 tracks that create open water surfaces, and there is also an area of eroded bare-peat surface on a dry
 133 fen.

134



135

136 **Fig. 1.** (a) Location of the study area in Tiksi, Yakutia, Russia, (b) Land-cover map with the
 137 chamber flux measurement points (dots) and the EC mast (x), and photos of the land-cover types:
 138 (c) lichen tundra with barren ground and patches of vegetation, (d) dwarf-shrub tundra, (e) bog, (f)
 139 wet and dry fen, (g) graminoid tundra, and (h) meadow by the stream. See Tuovinen et al. (2019)
 140 for the EC footprint climatology.

141

142

143

144

145 **Table 1.** Soil and vegetation characteristics of the land cover types (LCT) and their proportions in
 146 the EC impact area (90 % of the cumulative footprint).

LCT	Soil properties and plant taxa	Proportion (%) ²
Lichen tundra ¹	Mixture of vegetated patches, stones, and bare ground.	8 barren, 11 sparse vegetation

Lichens, e.g. genera *Thamnolia*, *Flavocetraria*, *Alectoria*, *Stereocaulon*, dwarf shrubs *Dryas octopetala*, *Vaccinium vitis-idaea*, *Salix polaris*, *Diapensia lapponica*, and forbs *Oxytropis* spp., *Astragalus* spp., *Pedicularis* spp., *Artemisia* spp., *Minuartia* sp.,

Dwarf-shrub tundra	Shallow organic layer on mineral soil ground Feather mosses, lichens, <i>Salix polaris</i> , <i>Vaccinium vitis-idaea</i> , <i>Vaccinium uliginosum</i> , <i>Dryas octopetala</i> , <i>Cassiope tetragona</i> , <i>Betula nana</i> , <i>Polygonum viviparum</i> , <i>Pedicularis</i> spp., <i>Carex</i> spp.	18
Meadow	Shallow organic layer on mineral soil ground <i>Calamagrostis</i> sp., <i>Festuca</i> sp., <i>Salix</i> spp. <i>Polygonum viviparum</i> , <i>Bistorta major</i> , <i>Polemonium</i> sp., <i>Valeriana</i> sp.	1.4
Graminoid tundra	Shallow peat layer on mineral soil ground Feather mosses, <i>Sphagnum</i> spp., <i>Carex</i> spp., <i>Eriophorum</i> spp., <i>Calamagrostis</i> spp., <i>Salix</i> spp., <i>B. nana</i> , <i>Saxifraga</i> spp., <i>Ranunculus</i> spp., <i>Bistorta major</i> , <i>Stellaria</i> sp., <i>Valeriana</i> sp., <i>Polemonium</i> sp., <i>Comarum palustre</i>	13
Bog	Dry hummock habitat at the tundra peatland <i>Sphagnum</i> spp., feather mosses, <i>Salix</i> spp., <i>Vaccinium uliginosum</i> , <i>Vaccinium vitis-idaea</i> , <i>Betula nana</i> , <i>Rhodendron tomentosum</i> , <i>Cassiope tetragona</i> , <i>Carex</i> spp., <i>Polygonum viviparum</i> ., <i>Stellaria</i> sp.	23
Dry fen	Intermediate wet tundra peatland habitat <i>Sphagnum</i> spp., <i>Carex</i> spp., <i>Salix</i> spp. <i>Saxifraga</i> spp., <i>Comarum palustre</i> , <i>Epilobium</i> spp., <i>Ranunculus</i> spp., <i>Pedicularis</i> spp., <i>Stellaria</i> sp.	10
Wet fen	Wet tundra peatland habitat with open pools <i>Brown mosses</i> , <i>Carex</i> spp., <i>Eriophorum</i> spp., <i>Ranunculus</i> sp., <i>Caltha palustris</i> , <i>Pedicularis</i> sp., <i>Saxifraga</i> sp.	15

147 ¹⁾ Combined the land cover types bare and lichen tundra LCTs defined in Juutinen et al. (2017),
 148 Mikola et al. (2018), and Tuovinen et al. (2019).²⁾ Proportion within the 90% coverage of the mean
 149 EC footprint area during the growing season of 2014 (Tuovinen et al. 2019).

150

151

152 2.2 CO₂ and CH₄ flux measurements

153 Fluxes of CO₂ and CH₄ were measured using static chambers equipped with a fan and set on pre-
 154 installed collars of 50 cm × 50 cm in area. The measurement points (collars) were set to cover the
 155 heterogeneity in land cover, and in each study year, there were 1–4 measurement points per each

156 LCT (Table 2). Most of the data were collected during a study campaign in July 15 – August 16,
 157 2014 (12 collars). The growing season had started earlier due to a warm period, and the daily mean
 158 air temperature stayed over 5 °C since July 5 (Fig. 2 and Tuovinen et al. 2019). The net ecosystem
 159 exchange of CO₂ (NEE) and ecosystem respiration of CO₂ in the dark (ER) were measured using
 160 transparent and opaque chambers (transparent chamber covered with a hood), respectively, allowing
 161 the partitioning of ecosystem gross photosynthesis (Pg) and ER. Fluxes of CH₄ were determined
 162 from closures of both transparent and opaque chambers, but because there was no difference
 163 between them when performed consecutively, the data from opaque chamber measurements were
 164 used for flux calculations. In addition, CH₄ fluxes were measured during shorter campaigns in 2012,
 165 2013, 2016, and 2019 (Table 2). These data also included the plots disturbed by vehicle tracks
 166 disturbance-plots and an eroded bare-peat surface, which were measured in 2019.

168 **Table 2.** Measurement periods, measured fluxes (CH₄, ER, NEE), and number of measurement
 169 points in each land cover type (LCT) across the study years.

	2012	2013	2014	2016	2019
LCT	Jul 18– 21	Jul 5–Sep 3	Jul 15–Aug 16	May 30, Aug 4–5, Sep 13–14	Aug 28–Sep 1
	CH ₄	CH ₄	ER, NEE, CH ₄	CH ₄	CH ₄
Wet fen (Vehicle track)	4	6	3	3	5 (2)
Dry fen (Bare peat)	2	4	3	3	2 (1)
Bog	2	3	1		1
Meadow	1	2	2		
Dwarf-shrub tundra	1		1	1	
Lichen tundra (snow ¹)		1	2	2 (2)	2

¹Measured only on May 30, 2016.

172 **Table 2.** Measurement periods, measured fluxes (CH₄, ER, NEE), and number of measurement
 173 points and observations (points, observations) in each land cover type (LCT) across the study years.

	2012	2013	2014	2016	2019
LCT	Jul 18–21	Jul 5–Sep 3	Jul 15–Aug 16	May 30, Aug 4–5, Sep 13–14	Aug 28–Sep 1
	CH ₄	CH ₄	ER, NEE, CH ₄	CH ₄	CH ₄

Wet fen	4,4	6,22	3,107	3,27	5,72
—Vehicle track					2,30
Dry fen	2,2	4,11	3,107	3,14	2,26
—Bare peat					1,15
Bog	2,2	3,7	1,36		1,13
Meadow	1,1	2,6	2,62		
Dwarf shrub tundra	1,1		1,36	1,1	
Lichen tundra		1,3	2,67	2,18	2,29
—Snow and ice [†]	-	-	-	2,2	-

[†]Measured only on May 30, 2016.

In 2012 and 2013, four air samples were taken from the chambers using syringes. The samples were stored in glass vials prior to the analysis. First, a vial was flushed with the sample and then filled to over-pressure. The samples were analyzed for CH₄ concentration using a TSVET 500-M gas chromatograph (Chromatek, Russia) with a flame ionization detector at the laboratory of the Voeikov Main Geophysical Observatory within a month from sampling. Each measurement was accompanied by calibration using standard gas mixtures with known CH₄ concentrations (the NOAA2004 scale). The vials were tested prior to the field sampling using a standard gas: after two weeks, the vials were still over-pressurized and the sample CH₄ concentrations were within ±3 ppb of the initial standard gas concentration. Since July 2014, CH₄ and CO₂ concentrations inside the chambers were recorded every second during closures of about 5 min using a gas analyzer (DLT-100, Los Gatos Research, Inc., San Jose, CA, USA) (see Fig. A2 for examples).

Gas fluxes between the ecosystem and the atmosphere were calculated from the phase of linear concentration change in the chamber head space over time, and accounting for temperature, volume, and atmospheric pressure. The concentration change during each chamber closure was evaluated visually for determining the closure start time and to remove cases showing nonlinearity due to leaks, ebullition, or saturation. The first data points were generally neglected when determining the slope of concentration change over time, and The linearity of the change was screened also on the basis of the cases with a linear concentration change had a the coefficient of determination of the fit (R^2). An $R^2 >$ greater than 0.9 was required, except for. For near-zero

194 fluxes cases smaller R^2 values were accepted to not ignore those cases. There were a few ebullition
195 cases at the vehicle track measurement points that had only sparse or no vegetation cover, and those
196 measurements were included in the final data. When determining the NEE fluxes measured using
197 the transparent chamber, the data were screened for variation in photosynthetically active photon
198 flux density (PPFD), measured during the chamber closure, and ~~a case the flux measurement was~~
199 rejected if the PPFD variation exceeded $100 \mu\text{mol m}^{-2} \text{s}^{-1}$ during the closure measurement.

200 The fluxes of CO_2 and CH_4 were also measured by the micrometeorological EC
201 method, which provides continuous data of the atmosphere-biosphere fluxes averaged on an
202 ecosystem scale. The EC system consisted of a three-dimensional sonic anemometer (USA-1,
203 METEK GmbH, Elmshorn, Germany), a closed-path CH_4 analyzer (RMT-200, Los Gatos Research,
204 Inc., San Jose, CA, USA), and a closed-path $\text{CO}_2/\text{H}_2\text{O}$ analyzer (LI-7000, LI-COR, Inc., Lincoln,
205 NE, USA). The fluxes were calculated as 30-min averages and processed using standard methods
206 (Aubinet et al. 2012). The EC measurement system and the post-processing procedures have been
207 presented in more detail by Tuovinen et al. (2019).

208 Supporting meteorological measurements including air temperature (T_{air}) (HMP,
209 Vaisala), soil temperature (T_{soil}) (IKES, Nokeval), PPFD (PQS1, Kipp & Zonen), and water table
210 level relative to the ground surface (WT) (8438.66.2646, Trafag) were collected by a Vaisala QML
211 datalogger as 30-min averages. We also present meteorological data for the period 2011–2019 to
212 relate the conditions during the measurement campaigns in ~~July 15–August 16, 2014, and the CH_4~~
213 ~~flux campaigns in~~ 2012, 2013, 2014, 2016, and 2019, to longer-term variations.

214 215 2.3 Vegetation and Topographic Wetness Index

216 On a site level, vegetation and soil characteristics were inventoried in plots assigned into a
217 systematic grid outside the area covered by the gas flux measurement points in 2014 (see Juutinen
218 et al. 2017; Mikola et al. 2018). The projection cover (%) of plant species and species groups, and
219 the mean canopy height of each species group were recorded. ~~Seven-Eight~~ species groups were

220 included in the inventory: *Sphagnum* mosses, feather mosses, brown mosses, dwarf shrubs, *Betula*
221 *nana*, *Salix* species, forbs, and graminoids. A subset of the plots was harvested, and vascular plant
222 leaves were scanned to determine the one-sided LAI ~~for to find an~~ empirical relationships between
223 LAI and %-cover and canopy height, which were used to estimate the LAI in the collars (see
224 Juutinen et al. 2017). In the collars, the projection cover and canopy height of each species group
225 were recorded weekly during the gas flux measurement campaign in July 15–August 16, 2014.
226 Because there were no observational vegetation data for the other years than 2014, the green
227 chromatic coordinate (GCC) calculated from digital photographs was used as a proxy for the
228 amount of green above-ground vascular plants (e.g. Richardson 2019). The GCC was calculated
229 from the digital numbers of red (R), green (G), and blue (B) color channels as the proportion of
230 green in the RGB images, $GCC = G/(R+G+B)$, of the vegetation inside the collars. The photographs
231 were taken at the time of measurements. We determined an empirical relationship between LAI and
232 GCC by using a data set of harvested plots with digital photographs and measured LAI data (n =
233 91). For the LAI estimation, we used a linear relationship ($R^2 = 0.46$, $p < 0.001$) between LAI and
234 GCC determined using the entire data set (see Fig. A3 for the data and equation).

235 To quantify the potential soil wetness at each measurement point, we calculated the
236 mean topographic wetness index (TWI) ~~value~~ based on a 2 m spatial resolution digital elevation
237 model (Mikola et al. 2018). To characterize differences between growing seasons as manifested by
238 vegetation greenness, the MODIS Normalized Difference Vegetation Index (NDVI) with 16-day
239 temporal and 500 m spatial resolution was calculated for a circular area with a 300 m radius from
240 the flux tower using Google Earth Engine (Gorelick et al. 2017). NDVI was derived for 2011–2019
241 to place the measurement years in the context of year-to-year variation in weather and plant growth.

243 2.4 Data analyses

244 When examining the role of the LCTs in CO₂ and CH₄ exchange, we applied the land cover
245 classification presented by Mikola et al. (2018). The data collected in July 15 – August 16, 2014

246 were used for examining gas exchange in relation to the variation in LAI, GCC, WT, and TWI
247 among the collars. The light-normalized Pg and NEE at PPFD = 800 $\mu\text{mol m}^{-2} \text{s}^{-1}$ (P_{g800} and
248 NEE_{800} , respectively), were estimated by fitting a hyperbolic response function of CO_2 vs PPFD
249 utilizing the ER and NEE flux data:

$$251 \quad NEE = ER - P_{g_{max}} \times \text{PPFD} / (\beta + \text{PPFD}), \quad (1)$$

252
253 where $P_{g_{max}}$ is the asymptotic maximum of photosynthetic [CO₂ uptake rates](#), and β is the half-
254 saturation PPFD. Fluxes of CH_4 are expressed as temporally averaged [for](#) each collar. We used
255 a sign convention where a positive [flux value](#) means net release to the atmosphere and a negative
256 [flux value](#) denotes net uptake by the ecosystem. Fluxes of CH_4 measured over all study years, 2012–
257 2019, were averaged for each LCT.

258 Regression analyses were used to test the relationships between gas flux estimates and
259 vascular LAI, GCC, WT, and TWI. All CH_4 flux data from the years 2012–[2014](#), 2016, and 2019
260 were used to quantify the mean growing season CH_4 flux for each LCT and examine the
261 relationship between CH_4 and GCC and TWI. To find the main factors and gradients in the plant
262 community, gas flux, and environmental variables data measured in the flux collars in 2014, we
263 performed a detrended correspondence analysis (DCA) of the species group data with [a](#) post-hoc fit
264 of environmental variables, including gas fluxes, WT, LAI, GCC, elevation, and thaw depth as
265 supplementary variables. The DCA was performed on logarithmically transformed, centered species
266 data (species or species groups) using Canoco 5 (Ter Braak and Šmilauer 2012).

267 We compared the LCT-specific flux estimates [obtained from](#)~~based on~~ the chamber
268 measurements with the estimates based on EC measurements [during](#)~~over~~ the same period ([July 15 –](#)
269 [August 16, 2014](#)). Partitioning of the EC-based CO_2 fluxes to Pg and ER and [the](#) estimates of P_{g800}
270 and NEE_{800} were calculated similarly to [those derived from the](#)~~that of~~ chamber data [using](#) (Eq. (1)).
271 The EC flux data were classified into five wind sectors (30–125°, 125–185°, 185–239°, 239–310°, 310–360°).

272 310–360°) based on the mean EC flux footprint, modeled for the growing [season](#) of 2014 by
273 Tuovinen et al. (2019). The sectors distinguished areas dominated by different LCTs, especially
274 tundra heaths and wetlands, and similarly those with a large and small vascular LAI. For each
275 sector, the footprint-weighted areal proportions of LCTs and mean vascular LAI were derived from
276 the ~~high-spatial-resolution~~ LCT and LAI maps (Mikola et al. 2018). For this comparison, sector
277 averages of Pg₈₀₀, ER, NEE₈₀₀, and CH₄ flux were calculated from the chamber data by weighting
278 the LCT-specific flux estimates with the above-mentioned LCT proportions in each sector. Because
279 there were no chamber measurement points within graminoid tundra, we applied wet fen (for CO₂)
280 and dry fen (for CH₄) flux estimates for the graminoid tundra based on the observed similarities in
281 LAI and soil wetness, respectively. Overall, graminoid tundra can be considered part of the fen
282 continuum in terms of soil characteristics ([notably](#) high organic content) and CH₄ exchange (Mikola
283 et al. 2018, Tuovinen et al. 2019).

284 Finally, to synthesize the CO₂ and CH₄ exchange variability across the tundra, we
285 upscaled the LCT-specific [average](#)-NEE₈₀₀, Pg₈₀₀, ER, and CH₄ flux (2014 data) [estimate averages](#)
286 to the 35.8 km² area surrounding our study site, for which a LCT map was produced by Mikola et
287 al. (2018).

288

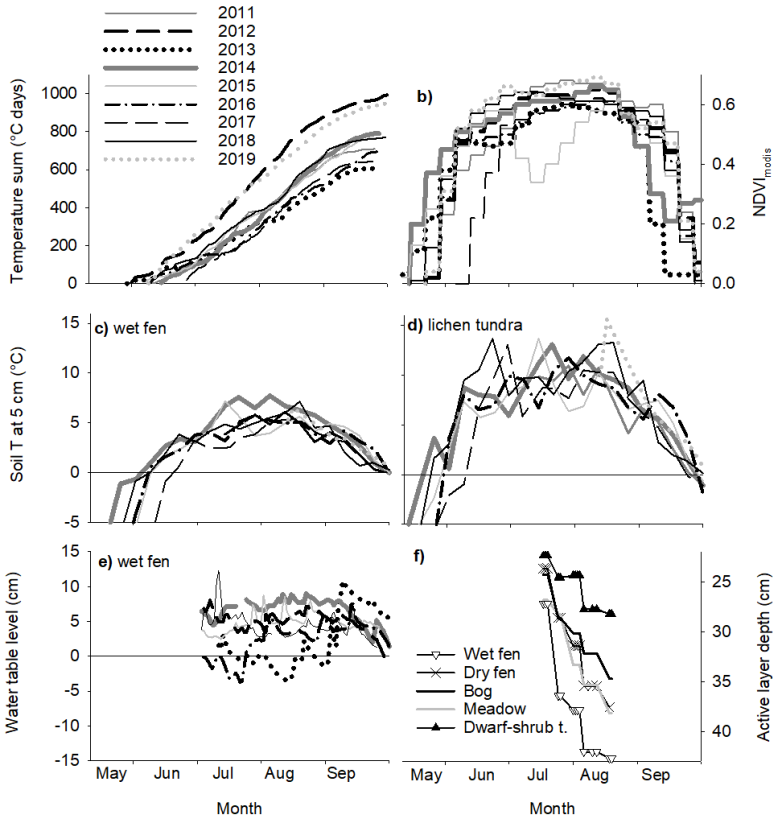
289 **3 Results**

290 *3.1 Environmental conditions*

291 In 2014, when we collected most of the flux data, temperature sum accumulation (with a 0 °C T_{air}
292 threshold) [took place at a](#) ~~was~~-near-average [rate](#) during the thaw period (the period when soil
293 surface temperature was continuously above 0 °C), but the spring and mid-growing season were
294 warmer than on average (Fig. 2a). The average air temperature was 15 °C during the gas flux
295 measurements. Accordingly, the MODIS NDVI showed an early start of greening (Fig. 2b), and
296 vegetation development had already started at the beginning of the measurement period. In 2011–
297 2019, which includes [sd all](#) the ~~other~~ CH₄ measurement years, the thaw period lasted for 74–124

298 days, creating a temperature sum range of 642–1003 °C days (Fig. 2a). Surface soils thawed
299 between May 28 and July 9 and froze again between September 21 and October 1. Among the
300 observation years, the years 2012 and 2019 had notably longer and warmer thaw periods than the
301 other years. The driest habitat, lichen tundra, with least snow accumulation, thawed 10–15 days
302 earlier than the other habitats, and had ~~an about-ca.~~ 3 °C higher soil temperature at the depth of 5
303 cm than ~~the~~ wet fen ~~at the depth of 5 cm~~ (Fig. 2c–d). Water table level, measured at a wet fen
304 location, showed only subtle interannual variation (Fig. 2e). In 2014, the active layer depth,
305 measured ~~over the measurement period~~ close to the collars during the flux measurement period, was
306 deepest in the end of August, reaching *ca.* 40 cm in wet fen, ~~and but remain~~ing < 30 cm in the ~~dry~~
307 dwarf-shrub tundra (Fig. 2f). Lichen tundra had rocks underneath the loose surface layer, which
308 made it impossible to measure the actual thaw depth.

309



310

311 **Fig. 2.** (a) Air temperature accumulation with the threshold T_{air} and surface T_{soil} and T_{air} of 0 °C, (b)
 312 seasonal dynamics of NDVI in the study area, (16-d MODIS data), (c) weekly means of soil
 313 temperature at a depth of 5 cm in wet fen and (d) in lichen tundra, (e) water-table level relative to
 314 the ground surface in wet fen, and (f) LCT-specific means of thaw depth in the measurement collars
 315 in 2014. Rocks in the ground prevented detecting the thaw depth of lichen tundra.

316

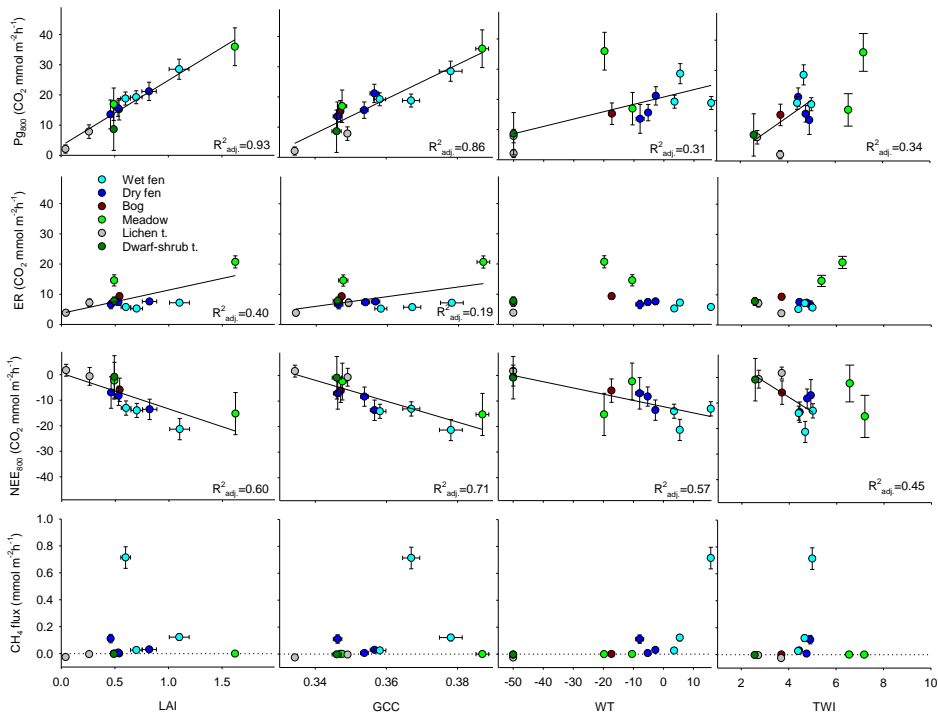
317 3.2 Exchange of CO_2 and CH_4

318 Among different LCTs, the estimates of P_{g800} varied from about 5 $mmol\ m^{-2}\ h^{-1}$ in the lichen tundra
 319 to 22 and 27 $mmol\ m^{-2}\ h^{-1}$ in the wet fen and meadow, respectively (Table 3a). P_{g800} was strongly
 320 and positively correlated with the vascular plant LAI and the greenness index GCC (Fig. 3). There
 321 was also a positive correlation between P_{g800} and both WT and TWI, possibly because the highest
 322 LAI occurred at the wet fen and meadow plots. However, the TWI values for the two meadow plots
 323 located on an elevated bank of the stream were disproportionately high in relation to the WT at

324 these plots, probably because of insufficient ~~spatial~~~~location~~ accuracy or an artefact ~~of~~ the digital
325 elevation model. Ecosystem respiration was highest in the two meadow plots, on average 18 mmol
326 $\text{m}^{-2}\text{h}^{-1}$. The relationship between ER and LAI was weaker than between Pg_{800} and LAI (Fig. 3).
327 NEE_{800} varied from about zero in the lichen tundra plots to a net CO_2 uptake of 16 $\text{mmol m}^{-2}\text{h}^{-1}$ in
328 the meadow and wet fen plots (Table 3a). NEE_{800} was more tightly linked to Pg_{800} than to ER and it
329 was correlated with LAI, GCC, WT, and TWI (Fig. 3).

330 There was substantial consumption of ~~the~~ atmospheric CH_4 in the barren tundra,
331 where the mean of all measured fluxes was $-0.018\text{ mmol m}^{-2}\text{h}^{-1}$, and in ~~the~~ vegetated lichen tundra
332 ~~with a~~ mean of $-0.005\text{ mmol m}^{-2}\text{h}^{-1}$ (Table 3c, Figs. 4 and 5). Minor consumption occurred in the
333 bog, meadow, and dwarf-shrub tundra plots (means ~~fluxes from~~ -0.0002 to -0.001 ~~± standard~~
334 ~~error~~ $0.0008\text{ mmol m}^{-2}\text{h}^{-1}$), while efflux to the atmosphere was observed in the dry fen (mean 0.04
335 $\text{mmol m}^{-2}\text{h}^{-1}$) and wet fen plots (means 0.05 and 0.16 $\text{mmol m}^{-2}\text{h}^{-1}$), respectively; Figs. 4 and
336 5). Fluxes were also high in ~~the~~ eroded bare-peat plot within the dry fen habitat and the vehicle-
337 track plots in wet fen (Table 3c).

338 ~~had equally high emissions as the fens (up to~~ $0.2\text{ mmol m}^{-2}\text{h}^{-1}$). Variation among the
339 plot means ~~of~~ CH_4 flux (Fig. 3 for 2014) ~~and~~ ~~LCT~~ means ~~of~~ (Fig. 5 for all years) CH_4 flux was
340 related to WT, and CH_4 emissions occurred when TWI was ~~greater than~~ $\rightarrow 4$. The two meadow plots
341 that showed net consumption of CH_4 had an unrealistically high TWI relative to their WT (see
342 above and Figs. 3 and 5). Variation in CH_4 fluxes was incoherently related to ~~the~~ variation in LAI
343 and GCC because of the high emission cases in plots with little vegetation, including the wettest
344 wet fen ~~plot~~, vehicle-track, and bare-peat plots (Fig. 5).



345

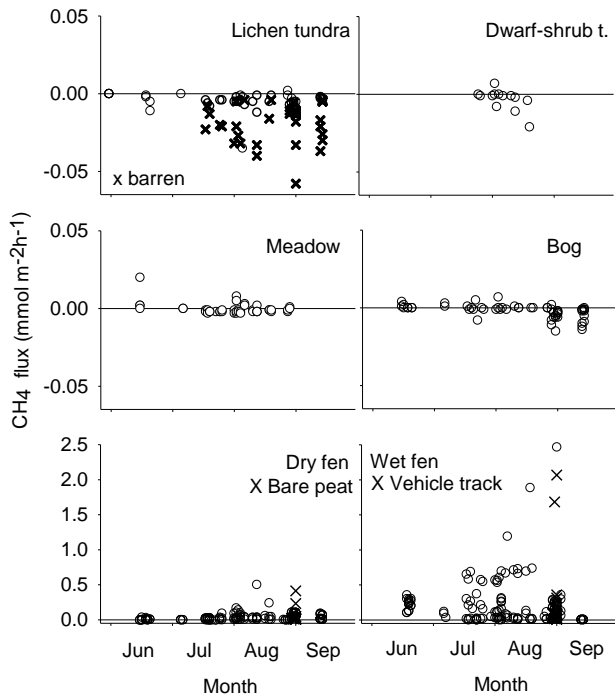
346

347 **Fig. 3.** Variation in the estimates of Pg₈₀₀, ER, and NEE₈₀₀ (Eq. 1) and collar means of CH₄ fluxes
 348 in relation to variation in the collar means of LAI, GCC, WT, and TWI in July 6–August 16, 2014.
 349 Error bars denote the standard error of estimate (n = 15 or 16 measurements per figure data
 350 point). Fitted regression lines and adjusted coefficients of determination (R²_{adj}) are included for the
 351 significant linear relationships. The two meadow plots were not included in the TWI regressions.

352

353

354

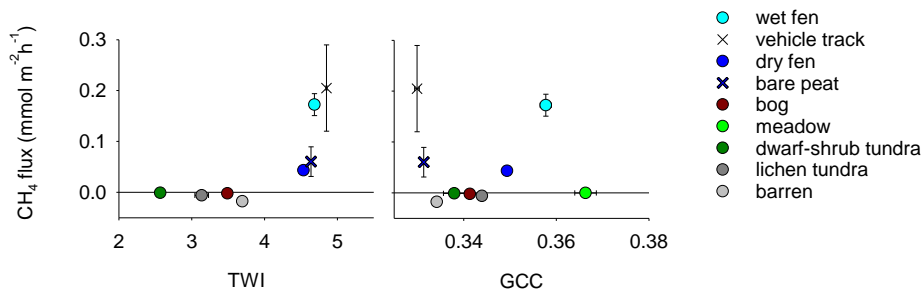


355

356 **Fig. 4.** Instantaneous CH_4 fluxes in each LCT. The data are a composite of all study years. Barren
 357 surfaces are indicated among the lichen tundra data. The eroded bare-peat and vehicle-track plots
 358 (\times) are plotted as part of the dry fen and wet fen data, respectively. Note that the panel groups have
 359 different y-axis scales.

360

361

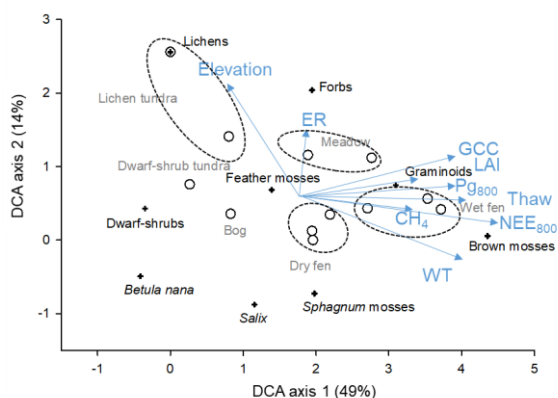


362

363 **Fig. 5.** LCT mean (\pm SE) CH_4 fluxes in relation to [the corresponding LCT](#) mean (\pm SE) TWI
 364 (excluding the meadow)- and [mean](#) GCC. -Data from years 2012–2019; [see Table 3c for the number](#)
 365 [of measurements.](#)-

366

367 The DCA ordination of species groups with a post-hoc fit of environmental variables
 368 (elevation, WT, thaw depth, LAI, GCC, and CO₂ and CH₄ exchange) showed that species
 369 distributed along a moisture gradient. Axis 1 explained 49 % of the variation in the species data and
 370 distinguished the wet and dry LCTs, i.e. from the wet fen to the lichen tundra (Fig. 6). Graminoids
 371 and brown mosses occurred in the wet end of the gradient, while evergreen dwarf-shrubs, *Betula*
 372 *nana*, and lichens occurred in the dry end of it. The barren plot (the other lichen tundra plot) with its
 373 negligible vegetation differed most from the other plots. Axis 2 explained additional 14 % of the
 374 variation in the species data (Fig. 6). The supplementary variables WT, vascular plant LAI, thaw
 375 depth, GCC, Pg₈₀₀, NEE₈₀₀, and CH₄ fluxes correlated positively with Axis 1 having post-hoc
 376 correlations (*r*) of 0.6–0.9, as derived from the DCA-weighted correlation matrix, while, in turn,
 377 plot's elevation and ER had positive correlations with Axis 2 (*r* = 0.8 and 0.4, respectively).



378 **Fig. 6.** DCA ordination diagram based on species (species groups) data from the measurement
 379 collars in 2014. The explained variation in the species data is indicated for the axes. In the plot,
 380 the scores are indicated for species groups (cross), sample plots (open symbols), and post-hoc
 381 fits of the supplementary variables (blue arrows, blue type) mean CH₄, Pg₈₀₀, ER, NEE₈₀₀, thaw
 382 depth (Thaw), water table relative to the ground surface (WT), green chromatic coordinate (GCC),
 383 vascular plant LAI, and elevation above sea level (Elevation). Land-cover types of the sample plots
 384 are indicated in grey type) and the plots assigned to each the same LCTs are circled.

385
 386
 387 In both the southern (125–185°) and south-western wind sectors (125–185° and 185–
 388 239°) wind sectors, vegetation mainly consisted of graminoids, as the LCTs dry fen, wet fen,
 19

389 graminoid tundra, and meadow comprised 80 % of the total EC footprint-weighted area (Fig. 7a).
390 The northern sector (310–360°) was characterized by lichen tundra and bare ground that accounted
391 for 68 % of the footprint-weighted LCT areas, while all the other LCTs covered less than 18 % in
392 total. The other wind direction sectors had more even LCT distributions. The differences between
393 the sectors were similar in the EC-based and spatially weighted chamber-based averages of CO₂
394 exchange (Fig. 7b–d). Both Pg₈₀₀ and NEE₈₀₀ were largest in the southern and south-western sectors
395 and clearly smallest in the barren–lichen tundra-dominated sector in the north. The chamber-based
396 estimates of CO₂ exchange were, however, lower: on average, Pg₈₀₀ was 57 %, ER 93 %, and
397 NEE₈₀₀ 44 % of the mean EC-based fluxes among the wind direction sectors.

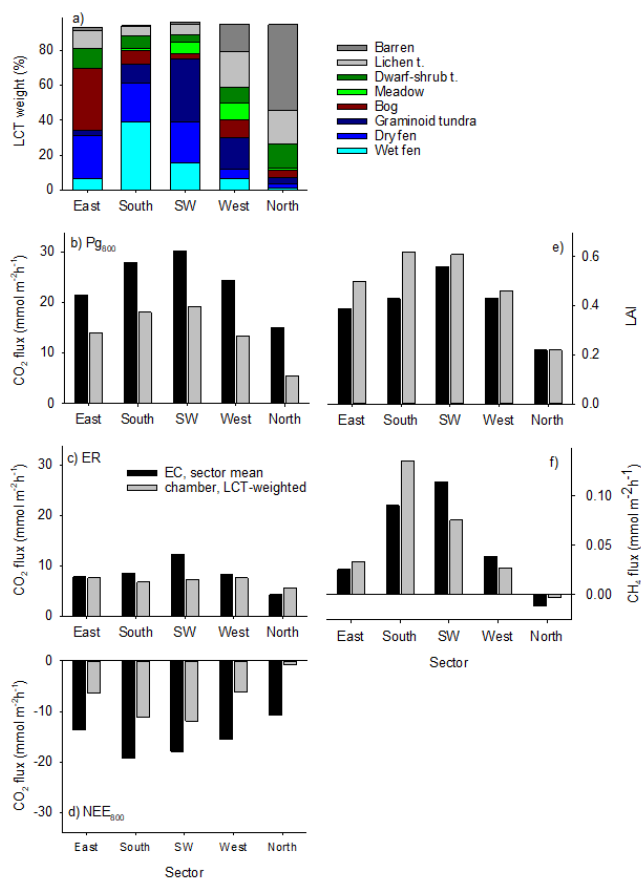
398 The southern and south-western wind sectors with abundant dry and wet fens and
399 graminoid tundra had clearly the largest CH₄ fluxes (Fig. 7f). The estimate based on chamber
400 measurements was 30 % and 50 % larger than the mean EC-based flux in the east sector (dominated
401 by dry fen and bog) and south sector (dominated by dry [fen](#) and wet fen), respectively. In contrast,
402 the chamber-based estimate was smaller than the EC flux for the other sectors, which were
403 dominated by graminoid tundra, lichen tundra, and barren ground. Both the EC- and chamber-based
404 measurements showed consumption of atmospheric CH₄ in the northernmost sector, of which
405 barren ground and lichen tundra covered 50 % and 20 %, respectively. The mean EC flux was three
406 times the chamber-based estimate.

407 Within the extended study area of 35.8 km², the LCT-weighted mean NEE₈₀₀ was -4.6
408 mmol m⁻² h⁻¹ (uptake relative to the atmosphere). The corresponding mean Pg₈₀₀ was 11 mmol m⁻²
409 h⁻¹, and [the mean](#) CH₄ flux [was](#) 0.05 mmol m⁻² h⁻¹ (Table 3a). Relative to their spatial cover (28 %
410 in total), wet and dry fens were disproportionally important for the landscape-level Pg₈₀₀, NEE₈₀₀,
411 and CH₄ emissions, because the fens contributed 47 % of total Pg₈₀₀ and 74 % of NEE₈₀₀, and were
412 the [dominant-largest](#) source of CH₄ [emission](#) (Table 3b). Consumption of CH₄ by barren and lichen
413 tundra, dwarf-shrub tundra, and meadow tundra soils contributed -9 % of the CH₄ balance, and the
414 barren ground dominated the sink. [Note-It should be noted that these data represents the growing](#)

415 [season conditions when both the CH₄ emissions and consumption of the atmospheric CH₄ were at](#)
 416 [their highest during the year the greatest due to higher temperatures, thawed soils and active](#)
 417 [vegetation growth.](#)

Formatted: Subscript

Formatted: Subscript



418 **Fig. 7.** Footprint-weighted mean contribution of each LCT to the EC measurements divided into
 419 wind direction sectors (a), and comparison of EC and chamber-based sector means of CO₂
 420 exchange (Pg₈₀₀, ER, and NEE₈₀₀) (b-d) vascular plant LAI (e), and CH₄ fluxes (f). The chamber-
 421 based data are weighted by the LCT proportions shown in panel a. All data were measured in 2014.
 422 Map of LAI (Tuovinen et al., 2019) and the LAI measured in the collars were used to estimate the
 423 EC- and chamber-related sector means, respectively, in panel e.

424
 425
 426 [Table 3. \(a\) Means, medians, and standard deviations \(sd\) of LCT specific CO₂ and CH₄ fluxes in](#)
 427 [2014 calculated from collar specific estimates \(CO₂\) or seasonal means \(CH₄\). There were 15 or 16](#)
 428 [data points per each collar and 1–3 collars per LCT \(see Table 2\). \(b\) Proportions of LCTs in](#)

429 landscape totals of area, and Pg₈₀₀, NEE₈₀₀, and CH₄ fluxes based on the LCT means (part a). (c)
 430 LCT specific means, medians, and standard deviations of CH₄ fluxes based on multiyear data (n is
 431 number of the observations).

a) LCT specific CO ₂ and CH ₄ fluxes in 2014 together with the landscape means (mmol m ⁻² h ⁻¹)									
LCT	Wet fen	Dry fen	Bog	Meadow	Dwarf-s. t.	Lichen t.	Barren	Gram. ¹	Mean ²
<u>Pg₈₀₀</u>									
mean	21.93	14.6	15.27	26.45	8.64	7.85	2.11	21.93	11.21
median	19.23	15.62		26.45					
sd	3.91	1.02		9.51					
<u>ER</u>									
mean	6.44	6.99	9.34	17.66	7.8	7.2	3.85	6.44	6.6
median	5.75	7.37		17.66					
sd	0.98	0.39		3.06					
<u>NEE₈₀₀</u>									
mean	-15.49	-7.61	-5.93	-8.79	-0.85	0.55	0.55	-15.49	-4.61
median	-13.99	-8.25		-8.79					
sd	3.39	0.64		6.45					
<u>CH₄</u>									
mean	0.29	0.05	0.0001	-0.001	-0.003	-0.005	-0.02	0.05	0.05
median	0.12	0.03		0.001					
sd	0.3	0.04		0.0003					

b) Proportions of LCTs in the landscape totals of area and CO ₂ and CH ₄ fluxes in 2014 (%)									
LCT	Wet fen	Dry fen	Bog	Meadow	Dwarf-s. t.	Lichen t.	Barren	Gram. ¹	
Area ³	16	12	9	0.4	27	11	15	3	
Pg ₈₀₀	32	15	12	1	21	5	7	7	
NEE ₈₀₀	55	19	12	1	5	-1	-2	11	
CH ₄	94	11	0	0	-2	-1	-6	3	

c) LCT specific CH ₄ fluxes during the study years 2012-2019 (mmol m ⁻² h ⁻¹)							
LCT	Wet fen (vehicle track)	Dry fen (bare peat)	Bog	Meadow	Dwarf-s. t.	Lichen t.	Barren
mean	0.17 (0.2)	0.04 (0.06)	-0.002	-0.0002	-0.001	-0.006	-0.018
median	0.04 (0.08)	0.03 (0.02)	-0.0008	-0.001	-0.0005	-0.005	-0.016
sd	0.29 (0.46)	0.06 (0.11)	0.004	0.004	0.007	0.005	0.013
n	183 (30)	118 (15)	58	43	29	37	47

432 ¹ Graminoid tundra contribution estimated using values for wet fen (CO₂) and dry fen (CH₄), ² Area-weighted
 433 mean. ³Water not showed.

434

435

436

437 Table 3. Land cover type distribution in the mapped 35.8 km² area (Mikola et al. 2018), spatially
 438 weighted and LCT specific means of Pg₈₀₀, ER, NEE₈₀₀, and CH₄, and proportions of LCTs in
 439 landscape totals of Pg₈₀₀, NEE₈₀₀, and CH₄ fluxes. Standard error of mean (SE) is shown for the
 440 LCT specific estimates. Data period: July 15—August 16, 2014.

LCT	Area (%)	Pg ₈₀₀ (mmol m ⁻² h ⁻¹)		ER (mmol m ⁻² h ⁻¹)		NEE ₈₀₀ (mmol m ⁻² h ⁻¹)		CH ₄ flux (mmol m ⁻² h ⁻¹)		Pg ₈₀₀ (%)	NEE ₈₀₀ (%)	CH ₄ flux (%)
Mean ¹		mean	SE	mean	SE	mean	SE	mean	SE			
Wet fen	16.4	21.9	2.5	6.4	0.7	-15.5	3.2	0.29	0.05	32.1	55.1	94.5
Dry fen	11.6	14.6	3.5	7.0	1.1	-7.6	4.6	0.05	0.01	15.1	19.1	11.2
Gram. t. ²	3.4	21.9	2.5	6.4	0.7	-15.5	3.2	0.05	0.01	6.7	11.4	3.3
Bog	9.1	15.3	3.6	9.3	1.0	-5.9	4.6	0.0001	0.0005	12.4	11.7	0.03
Meadow	0.4	26.4	5.8	17.7	1.9	-8.8	7.7	-0.001	0.0004	0.9	0.8	-0.01
Dwarf s. t.	27.4	8.6	7.0	7.8	1.3	-0.8	8.3	-0.003	0.0015	21.1	5.0	-1.8
Lichen t.	11.1	5.0	2.2	5.5	1.3	0.5	3.5	-0.005	0.001	4.9	-1.3	-1.1
Barren	15.3	5.0	1.4	5.5	1.0	0.5	2.3	-0.020	0.003	6.8	-1.8	-6.1
Water	5.3	NA	-	NA	-	NA	-	NA	-	-	-	-

¹area-weighted mean, ²Graminoid tundra fluxes estimated using values for wet fen (CO₂) and dry fen (CH₄)

Formatted: English (United States)

4 Discussion

The studied tundra site in Tiksi in northeastern Siberia has heterogeneous land cover, which is reflected as equally heterogeneous CO₂ and CH₄ exchange. We found that the LAI of vascular plants was a robust predictor of Pg₈₀₀ and NEE₈₀₀ across the LCTs. On the one hand, ~~due to the distribution of species and LAI,~~ the tundra wetlands had a disproportionate role in the landscape-level CO₂ uptake capacity. The fens also dominated the landscape's CH₄ emissions. On the other hand, our results highlight the ~~high-substantial~~ CH₄ consumption ~~rates of the atmospheric CH₄~~ within the dry tundra areas, ~~particularly in barrens.~~ The ~~CH₄ consumption of the atmospheric CH₄~~ by dry tundra ~~contributed was~~ -9 % of the total CH₄ balance ~~estimated for within~~ this landscape ~~from the data collected during the growing season,~~ ~~and the consumption rate of the barren was much higher than in other dry tundra habitats.~~ This finding is in agreement with other studies and suggest distinguishing non-vegetated dry tundra habitats when upscaling ~~plot-scale~~ CH₄ fluxes (Table 4). In Tiksi, the barren was characterized by sand and rocks underlain by chists (Fig. A1). The consumption of CH₄ was smaller ~~if when if~~ the sand and stones were partly covered with vegetation ~~and, in lichen tundra, with a thin organic layer~~ (Figs. 5 and A1). ~~Note, that the balance estimate represents only growing season conditions.~~

Formatted: Font: (Default) Times New Roman, 12 pt, Bold

Formatted: Subscript

459 The land-cover categorical approach serves to distinguish the basic features of spatial
460 variation in CO₂ and CH₄ fluxes, and the extreme ends of the moisture and vegetation
461 gradients from barren to wet fen are clearly distinguishable, also in terms of CO₂ and CH₄ exchange
462 (Fig. 6). Overall, microrelief, moisture gradient, vegetation types, and ecosystem functions are
463 connected. For instance, Barren-barren areas are wind swept and thus having minimal snow
464 accumulation, while in wet depressions snow accumulation further increases soil moisture (Fig. 6;
465 Callaghan et al. 2011). Nevertheless, the spatial extrapolation of fluxes, however, is here clearly
466 sensitive to a small number of chamber measurement points as there is large within-LCT variation
467 in fluxes and LAI, as observed in the wet fen and meadow data, which originates from the plot to
468 plot variation in LAI. Moreover, the LCTs share common features and form a continuum as
469 shown by the DCA ordination (Fig. 6). Mikola et al. (2018) used a larger soil and vegetation data
470 set from Tiksi and also found that the neighboring LCTs overlapped in terms of soil and plant
471 attributes properties and vegetation. Despite the limited number of observations, our conclusions
472 drawn from the chamber data are corroborated by the temporally matching section of EC data,
473 which show high similarity to the chamber data (Fig. 7). Furthermore, the statistical analysis of EC
474 data by Tuovinen et al. (2019) showed that it is possible to find significant differences between
475 different LCT categories representing high and low CH₄ emitters and CH₄ sinks. However, for
476 spatial modeling of ecosystem functions, maps of key variables, such as LAI and WT, that drive
477 CO₂ and CH₄ exchange would be preferable to categorical LCT classification (Räsänen et al. 2021).

478 The spatial pattern of the growing season Pg₈₀₀ and NEE₈₀₀ was strongly related to the
479 corresponding pattern of the LAI of vascular plants (Figs. 3 and 4). Hence, the abundance of
480 graminoid (Cyperaceae and Poaceae) vegetation was associated with a large NEE₈₀₀, which varied
481 from near zero in lichen tundra up to -25 mmol m⁻² h⁻¹ in wet fen. Ecosystem respiration had a
482 smaller role than Pg in determining NEE, but we note that our data cover only a section of the
483 growing season with warmer temperatures and half to full-grown vegetation. The importance of
484 ER is likely to be different when considering the full annual balance (e.g., Hashemi et al. 2021).

485 While our data represent only the growing season, a similar relationship has also been found
486 between the annual NEE and LAI at a tundra site with a mixture of wet and dry tundra in
487 northeastern Europe (Marushchak et al. 2013), in a multi-site EC study in Alaskan tundra
488 (McFadden et al. 2003), in Canadian low arctic tundra wetlands (Lafleur et al. 2012), and across
489 tundra sites (Street et al. 2007; Shaver et al. 2007).

490 The magnitude of P_{g800} and NEE_{800} in the fen and meadow plots of this study were
491 similar to the maximum P_g and NEE found in [a](#) tundra wetland in Seida in northeastern Europe
492 (Marushchak et al. 2013), at low tundra wetland sites in eastern Canada (Lafleur et al. 2012), and at
493 a wetland-dominated but more continental site (with an equally long growing season) in
494 northeastern Siberia (van der Molen et al. 2007). The vegetation and P_{g800} of lichen tundra and
495 dwarf-shrub tundra in our study resembled those observed within the polygon rim habitat of the
496 polygon tundra in the Lena River delta, while those of meadow, dry fen, and wet fen resembled the
497 wet polygon center habitats (Eckhardt et al. 2019). In our study, the [spatial](#) variation of ecosystem
498 respiration resulted from the variation in vascular plant LAI, soil organic content, and water
499 saturation: the highest ER occurred in [the](#) mineral soil meadow [plots](#) with [a](#) high LAI, suggesting
500 substantial autotrophic respiration, and likely deep rooting and large root biomass contributing to
501 ~~the~~ ecosystem respiration (Fig. 3).

502 Our chamber-based estimate of the average CH_4 flux within the 35.8 km² upscaling area
503 was 0.05 mmol m⁻² h⁻¹, which is close to 0.04 mmol m⁻² h⁻¹ obtained by Tuovinen et al. (2019), who
504 combined EC data with footprint modeling to statistically determine LCT group-specific CH_4
505 fluxes. Within this upscaling area, we estimate that 28 % of the area emitted CH_4 , while the other
506 habitats either consumed atmospheric CH_4 (barren and lichen tundra, dwarf-shrub tundra, meadow)
507 or were close to neutral ([bog](#)) relative to the atmosphere (Fig. 4, Table [3a-b](#)). The relationship
508 between [the](#) vascular plant LAI and CH_4 flux was confused by the occurrence of large CH_4 fluxes in
509 plots with little or no vegetation. Those ~~fluxes were observed~~~~deases occurred~~ at the wettest fen plot
510 and [the](#) bare-peat and vehicle track plots (Figs. [43-5](#)). ~~HA~~ [high](#) LAI, [a](#) high WT , and [a](#) high CH_4

511 emissions systematically co-occurred in wet fen (Fig. 6). In addition, [in the bare-peat and vehicle-](#)
512 [track plots](#), erosion or [anthropogenic](#) disturbance may have created CH₄ flux hotspots due ~~to the~~
513 ~~occurrence of~~ permafrost scars, water saturation, and recently thawed organic matter (e.g., Bubier et
514 al. 1995, McCalley et al. 2014, Wickland et al. 2020). These are small-scale landscape features,
515 while ~~in on~~ a larger scale, our data encourage applying indices of wetness and vegetation as a means
516 of CH₄ flux upscaling in a tundra environment.

517 The recognition of CH₄ consuming tundra habitats is important for accurately estimating
518 the net CH₄ balance of tundra. The substantial uptake of atmospheric CH₄ by lichen tundra (here a
519 mixture of bare ground and sparse vegetation) in Tiksi was inferred by Tuovinen et al. (2019) based
520 on a source allocation analysis of EC data: the average flux of the consuming area was estimated at
521 -0.03 mmol m⁻² h⁻¹, which corresponded to -22 % of the total upscaled CH₄ ~~balance flux~~. In this
522 study, the average seasonal CH₄ ~~flux uptake~~ was -0.02 mmol m⁻² h⁻¹ in the barren tundra and an
523 order of magnitude lower in meadow ~~and dwarf-shrub tundra~~. ~~Our upscaling exercise suggested~~
524 ~~a CH₄ sink that corresponded -9 % of the regional CH₄ balance~~. This difference [between the](#)
525 ~~estimates may likely~~ originates from the LCT-weighting and the small sample of the chamber-based
526 ~~data estimate~~ and, in general, demonstrates the inherent sensitivity involved in upscaling of fluxes of
527 opposite direction.

528
529 [Table 4. Summary of reported CH₄ fluxes in mineral soil dry tundra.](#)

Location	Habitat type	Mean	Min	Max	Reference
(μmol m⁻² h⁻¹)					
Narsarsuaq, Greenland	low elevation heath vegetation	-1.2	-4.0	-0.2	St Pierre et al. 2019
Narsarsuaq, Greenland	high elevation heath vegetation	-2.6	-11.9	3.6	St Pierre et al. 2019
Disko Island, Greenland	low elevation heath vegetation	-3.8	-12.1	-1.1	St Pierre et al. 2019
Disko Island, Greenland	high elevation heath vegetation	-3.5	-12.1	-1.3	St Pierre et al. 2019
Tierra del Fuego, Argentina	alpine tundra	0.5	-16.6	10.3	Sá et al. 2019
Disko Island, Greenland	dry tundra heath¹	-4.0	-4.4	-2.5	D'Imperio et al. 2017
Disko Island, Greenland	bare ground¹	-9.0	-15.0	-3.8	D'Imperio et al. 2017
Disko Island, Greenland	Betula nana and Salix sp. heath	-4.0			Christiansen et al. 2014
Axel Heiberg Island, CA	vegetated ice-wedge polygon		-2.7	-0.3	Lau et al. 2015
Lake Hazen, Ellesmere I., CA	polar desert²	-3.6	-7.0	0.0	Emmerton et al. 2014
Zackenber Valley, Greenland	moist tundra	-3.1	-7.0	-2.0	Jørgensen et al. 2014

Zackenber Valley, Greenland	dry tundra & barren ground	-7.0	-16.0	-4.0	Jørgensen et al. 2015
Zackenber Valley, Greenland	tundra heath	-1.3	-6.0	0.0	Christensen et al. 2000
Okse Bay, Ellesmere I., CA	polar desert ³	-0.5			Brummel et al. 2014
Petterson R., Ellesmere I., CA	polar desert ³	-0.04			Brummel et al. 2014
Dome, Ellesmere I., CA	polar desert ³	-0.5			Brummel et al. 2014
BAWLD-CH ₄ Synthesis	dry tundra		-2.9	5.2	Kuhn et al. 2021
BAWLD-CH ₄ Synthesis	boreal forest		-2.6	-0.5	Kuhn et al. 2021
Tiksi, RU	Barren & lichen tundra ⁴	-29			Tuovinen et al. 2019
Tiksi, RU	lichen tundra mean	-11.3	-57.9	-0.4	This study
Tiksi, RU	barren	-18.1	-57.9	-3.0	This study
Tiksi, RU	vegetated	-6.0	-34.7	-0.4	This study
Tiksi, RU	meadow	-1.0	-21.1	24.5	This study
Tiksi, RU	dwarf-shrub tundra	-0.2	-2.9	20.3	This study
Tiksi, RU	bog	-2.1	-14.8	6.6	This study

¹⁾ Mean estimated from a figure, ²⁾ minimum and maximum estimated from a figure, ³⁾ three day measurement, ⁴⁾ estimated from EC measurements with a statistical model.

High consumption of atmospheric CH₄ in barrens is associated with the high affinity methanotrophs (Emmertson et al. 2014, Jørgensen et al. 2014, D’Imperio et al. 2017, St Pierre et al. 2019). ~~In our summary of the CH₄ fluxes in mineral-rich dry tundra (Table 4) shows that,~~ the consumption ~~rates in Tiksi values of this study and Tuovinen et al. (2019) are higher than those observed elsewhere, the highest, and maybe~~ This may be due to a local feature associated with the parent material of the ground ~~in Tiksi~~. Similar rates, however, have been ~~observed in~~ recorded at other dry tundra sites with little or no vegetation. For instance, on Disko Island, Greenland, which consists of similar land cover types to Tiksi, ~~uptake of CH₄ uptake~~ by bare ground was -0.005–0.01 mmol m⁻² h⁻¹ during the growing season, while a mean ~~flux uptake~~ of -0.003–0.004 mmol m⁻² h⁻¹ was observed in dry tundra heath (D’Imperio et al. 2017). These consumption rates associated with tundra barrens and high-affinity methanotrophs can be even higher than those measured on north-boreal forest soils (e.g. for instance, -0.01 mmol m⁻² h⁻¹, Lohila et al. 2016).

~~Table 4. Summary of reported consumption rates of atmospheric CH₄ fluxes in mineral soil dry tundra. Note unit is μmol m⁻² h⁻¹.~~

Location	Habitat type	Mean	Min	Max	Reference
----------	--------------	------	-----	-----	-----------

		$(\mu\text{mol}\cdot\text{m}^{-2}\cdot\text{h}^{-1})$			
Narsarsuaq, Greenland	low elevation heath vegetation	-1.2	-4.0	-0.2	St Pierre et al. 2019
Narsarsuaq, Greenland	high elevation heath vegetation	-2.6	-11.9	3.6	St Pierre et al. 2019
Disko Island, Greenland	low elevation heath vegetation	-3.8	-12.1	-1.1	St Pierre et al. 2019
Disko Island, Greenland	high elevation heath vegetation	-3.5	-12.1	-1.3	St Pierre et al. 2019
Tierra del Fuego, Argentina	alpine tundra	0.5	-16.6	10.3	Sá et al. 2019
Disko Island, Greenland	dry tundra heath ¹	-4.0	-4.4	-2.5	D'Imperio et al. 2017
Disko Island, Greenland	bare ground ¹	-9.0	-15.0	-3.8	D'Imperio et al. 2017
Disko Island, Greenland	<i>Betula nana</i> and <i>Salix</i> sp. heath	-4.0			Christiansen et al. 2017
Axel Heiberg Island, CA	vegetated ice wedge polygon		-2.7	-0.3	Lau et al. 2015
Lake Hazen, Ellesmere I., CA	polar desert ²	-3.6	-7.0	0.0	Emmerton et al. 2014
Zaackenber Valley, Greenland	moist tundra	-3.1	-7.0	-2.0	Jørgensen et al. 2014
Zaackenber Valley, Greenland	dry tundra & barren ground	-7.0	-16.0	-4.0	Jørgensen et al. 2015
Zaackenber Valley, Greenland	tundra heath	-1.3	-6.0	0.0	Christensen et al. 2000
Okse Bay, Ellesmere I., CA	polar desert ³	-0.5			Brummel et al. 2014
Petterson R., Ellesmere I., CA	polar desert ³	-0.04			Brummel et al. 2014
Dome, Ellesmere I., CA	polar desert ³	-0.5			Brummel et al. 2014
BAWLD-CH ₄ Synthesis	dry tundra		-2.9	5.2	Kuhn et al. 2021
BAWLD-CH ₄ Synthesis	boreal forest		-2.6	-0.5	Kuhn et al. 2021
Tiksi, RU	Barren & lichen tundra ⁴	-2.9			Tuovinen et al. 2019
Tiksi, RU	lichen tundra-mean	-11.3	-57.9	-0.4	This study
Tiksi, RU	—barren	-18.1	-57.9	-3.0	This study
Tiksi, RU	—vegetated	-6.0	-34.7	-0.4	This study
Tiksi, RU	meadow	-1.0	-21.1	24.5	This study
Tiksi, RU	dwarf shrub tundra	-0.2	-2.9	20.3	This study
Tiksi, RU	bog	-2.1	-14.8	6.6	This study

Formatted: Font: Italic

548 ¹⁾ mean estimated from a figure, ²⁾ minimum and maximum estimated from a figure, ³⁾ one three day
549 measurement, ⁴⁾ estimated from EC measurements with a statistical model.

550

551 5 Conclusions

552 Our results provide new observations of carbon exchange for the prostrate dwarf shrub tundra sub-
553 zone, which covers a substantial area of the Arctic. These data augment the knowledge on the
554 functional diversity, namely the distribution of different land-cover types and their emission
555 factors, across the vast arctic tundra and will lend support to bottom-up and top-down
556 extrapolations across the Arctic. Graminoid vegetation that favored the wet and moist habitats, such
557 as wet fens, was characterized by large CO₂ uptake and CH₄ emissions. In addition, our data
558 support the observation of notable consumption of atmospheric CH₄ in barren tundra that has

559 substantial coverage across the Arctic. The heterogeneity of landscape and the related large spatial
560 variability of CO₂ and CH₄ fluxes observed in this study encourage to monitor the Arctic sites for
561 changes in habitat type distribution. Such changes can include the forming of meadows and wet
562 fens and appearance of new vegetation communities, such as erect shrubs, that benefit [from](#)
563 warming-induced changes in thaw depth and soil wetness. The spatial extrapolation based on a
564 small number of measurement points involves inherent uncertainty but still allowed us to identify
565 key relationships between CO₂ and CH₄ fluxes and vegetation and moisture features, which can be
566 utilized in more robust upscaling studies that make use of EC measurements.

567

568 *Data availability.* The flux data used in this study can be accessed via the Zenodo data repository
569 and from the PI: Juutinen, Sari. (2022). Dataset for a manuscript entitled Variation in CO₂ and CH₄
570 Fluxes Among Land Cover Types in Heterogeneous Arctic Tundra in Northeastern Siberia [Data
571 set]. Zenodo. <https://doi.org/10.5281/zenodo.5825705>

572

573 *Author contributions*

574 TL, MA, and SJ designed the study. TL, MA, and AM took care of the overall site governance and
575 maintenance. VI, ML, TL, JM, JN, EV, TL, TV, and MA conceived the field measurements of CO₂
576 and CH₄, vegetation, and environmental variables. In addition, ML calculated green chromatic
577 coordinates, and MA and J-PT postprocessed the EC data and J-PT modeled the footprint and
578 estimated footprint LCT fractions. AR and TV processed and modelled the landcover data and
579 estimated TWI and NDVI for the plots and area. SJ compiled the chamber flux data and conducted
580 the data analyses and spatial extrapolations and wrote the manuscript with contributions from all co-
581 authors.

582

583 *Competing interests*

584 The authors declare that they have no conflict of interest.

585

586 *Acknowledgements*

587 We thank G. Chumachenko, O. Dmitrieva, and E. Volkov at the Tiksi Observatory and the
588 Yakutian Hydrometeorological Service for their kind assistance in carrying out and organizing the
589 field campaigns and Lauri Rosenius for assistance in the field work. This study was financially
590 supported by the Academy of Finland, projects “Greenhouse gas, aerosol and albedo variations in
591 the changing Arctic” (project no. 269095), “Carbon balance under changing processes of Arctic and
592 subarctic cryosphere” (project no. 285630), “Constraining uncertainties in the permafrost-climate
593 feedback” (project no. 291736) and “Carbon dynamics across Arctic landscape gradients: past,
594 present and future” (project no. 296888); the European Commission, FP7 project “Changing
595 permafrost in the Arctic and its global effects in the 21st century (PAGE21, project no. 282700”;
596 and the Nordic Council of Ministers, DEFROST Nordic Centre of Excellence within NordForsk.

597 [We sincerely thank two anonymous reviewers for their time and insightful suggestions.](#)

598

599 **References**

- 600 AARI: Archive of Tiksi standard meteorological observations (1932–2016), Russian Federal
601 Service for Hydrometeorology and Environmental Monitoring, St Petersburg, Russia,
602 available at: http://www.aari.ru/resources/d0024/archive/description_e.html, last
603 access: 13 September 2018.
- 604 Aurela, M., Laurila, T., and Tuovinen, J-P.: The timing of snow melt controls the annual CO₂
605 balance in a subarctic fen, *Geophysical Research Letters* 31, L16119,
606 doi:10.1029/2004GL020315, 2004.
- 607 Brummel, M.E., Farrell, R.E., Hardy, S.P., and Siciliano, S.D., Greenhouse gas production and
608 consumption in High Arctic deserts, *Soil Biology and Biochemistry*, 68, 158–165,
609 <https://doi.org/10.1016/j.soilbio.2013.09.034>, 2014.

610 Bartlett, K. B., and Harriss, R. C., Review and assessment of methane emissions from wetlands.
611 Chemosphere, 26, 261–320, 1993.

612 Bubier, J.L., Moore, T.R., Bellisario, L., Comer, N.T., and Crill, P.M: Ecological controls on
613 methane emissions from a northern peatland complex in the zone of discontinuous
614 permafrost, Manitoba, Canada. Global Biogeochemical Cycles 9. 455–470, 1995.

615 Callaghan, T.V., Johansson, M., Brown, R.D. et al. Multiple Effects of Changes in Arctic Snow
616 Cover, 2011, AMBIO 40, 32–45 (2011). <https://doi.org/10.1007/s13280-011-0213-x>

617 Chen, L., Aalto, J., and Luoto, M.: Significant shallow–depth soil warming over Russia during the
618 past 40 years. Global and Planetary Change, 197, 103394,
619 doi.org/10.1016/j.gloplacha.2020.103394, 2021.

620 Christensen, T. R., Friberg, T., Sommerkorn, M., Kaplan, J., Illeris, L., Soegaard, H., Nordstroem,
621 C., and Jonasson, S., Trace gas exchange in a high-Arctic valley: 1. Variations in CO₂
622 and CH₄ Flux between tundra vegetation types, Global Biogeochemical Cycles, 14,
623 701– 713, [doi:10.1029/1999GB001134](https://doi.org/10.1029/1999GB001134), 2000.

624 Christiansen, J.R., Romero, A.J.B., Jørgensen, N.O.G., Glaring, M.A., Jørgensen, C.J., Berg, L.K.,
625 Elberling, B. Methane fluxes and the functional groups of methanotrophs and
626 methanogens in a young Arctic landscape on Disko Island, West Greenland,
627 Biogeochemistry, 122, 15–33, 2014.

628 D’Imperio, L., Skov Nielsen, C., Westergaard-Nielsen, A., Michelsen, A., and Elberling, B.:
629 Methane oxidation in contrasting soil types: responses to experimental warming with
630 implication for landscapeintegrated CH₄ budget. Global Change Biology 23, 966–976,
631 [doi: 10.1111/gcb.13400](https://doi.org/10.1111/gcb.13400), 2017.

632 Eckhardt, T., Knoblauch, C., Kutzbach, L., Holl, D., Simpson, G., Abakumov, E., and Pfeiffer, E-
633 M.: Partitioning net ecosystem exchange of CO₂ on the pedon scale in the Lena River
634 Delta, Siberia. Biogeosciences 16, 1543–1562, [doi:10.5194/bg-16-1543-2019](https://doi.org/10.5194/bg-16-1543-2019), 2019.

Formatted: Subscript

Formatted: Subscript

Formatted: Subscript

635 Emmerton, C.A., St Louis, V.L., Lehnerr, I., Humphreys, E.R., Ryzd, E., Kosolofski, H.R. The net
636 exchange of methane with high Arctic landscapes during the summer growing season.
637 *Biogeosciences*, 11, 3095–3106, 2014.

638 Euskirchen, E.S., Bret-Harte, M.S., Shaver, G.R., Edgar, C.W., and Romanovsky, V.E.: Long-Term
639 Release of Carbon Dioxide from Arctic Tundra Ecosystems in Alaska. *Ecosystems* 20,
640 960–974, doi: 10.1007/s10021-016-0085-9, 2017.

641 Gorelick, N., Hancher, M., Dixon, M., Ilyushchenko, S., Thau, D., and Moore, R.: Google Earth
642 Engine: Planetary-scale geospatial analysis for everyone. *Remote Sensing of*
643 *Environment*, 202, 18-27, doi.org/10.1016/j.rse.2017.06.031, 2017.

644 Hashemi, J., Zona, D., Arndt, K.A., Kalhori, A., and Oechel, W.C.: Seasonality buffers carbon
645 budget variability across heterogeneous landscapes in Alaskan Arctic Tundra.
646 *Environ. Res. Lett.* in press <https://doi.org/10.1088/1748-9326/abe2d1>, 2021.

647 Humphreys, E.R. and Lafleur, P.M.: Does earlier snowmelt lead to greater CO₂ sequestration in two
648 low Arctic tundra ecosystems? *Geophysical Research Letters* 38, L09703,
649 doi:10.1029/2011GL047339, 2011.

650 IPCC Summary for Policymakers in *Climate Change 2013: The Physical Science Basis* (eds
651 Stocker, T. F. et al.) 3–29, Cambridge Univ, Press, 2013.

652 Jørgensen, C.J., Lund Johansen, K.M., Westergaard-Nielsen, A., and Elberling, B.: Net regional
653 methane sink in High Arctic soils of northeast Greenland. *Nature Geoscience* 8, doi:
654 10.1038/NGEO2305, 2014.

655 Juutinen, S., Virtanen, T., Kondratyev, V., Laurila, T., Linkosalmi, M., Mikola, J., Nyman, J.,
656 Räsänen, A., Tuovinen, J-P., and Aurela, M.: Spatial variation and seasonal dynamics
657 of leaf-area index in the arctic tundra – implications for linking ground observations
658 and satellite images. *Environmental Research Letters* 12, doi.org/10.1088/1748-
659 9326/aa7f85, 2017.

Formatted: Subscript

660 Kuhn, M. A., Varner, R. K., Bastviken, D., Crill, P., MacIntyre, S., Turetsky, M., Walter Anthony,
661 K., McGuire, A. D., and Olefeldt, D.: BAWLD-CH₄: a comprehensive dataset of
662 methane fluxes from boreal and arctic ecosystems, *Earth Syst. Sci. Data*, 13, 5151–
663 5189, <https://doi.org/10.5194/essd-13-5151-2021>, 2021.

664 Lau, M.C.Y., Stackhouse, B.T., Layton, A.C., Chauhan, A., Vishnivetskaya, T.A., Chourey, K.,
665 Ronholm, J., Myktyczuk, N.C.S., Bennett, P.C., Lamarche-Gagnon, G., Burton, N.,
666 Pollard, W.H., Omelon, C.R., Medvigy, D.M., Hettich, R.L., Pfiffner, S.M., Whyte,
667 L.G., and Onstott, T.C.: An active atmospheric methane sink in high Arctic mineral
668 cryosols. *The ISME Journal* 9, 1880–1891, doi:10.1038/ismej.2015.13, 2015.

669 Lafleur, P.M., Humphreys, E.R., St. Louis, V.L., Myklebust, M.C., Papakyriakou, T., Poissant, L.,
670 Barker, J.D., Pilote, M., and Swystun, K.A.: Variation in Peak Growing Season Net
671 Ecosystem Production Across the Canadian Arctic. *Environmental Science and
672 Technology* 46, 7971–7977, doi.org/10.1021/es300500m, 2012.

673 Lara, M.J., McGuire, A.D., Euskirchen, E.S., Genet H., Yi, S., Rutter, R., Iversen, C., Sloan, V.,
674 and Wullschleger, S.D.: Local-scale Arctic tundra heterogeneity affects regional-scale
675 carbon dynamics- *Nature Communications* 11, 4925, doi:10.1038/s41467-020-18768-
676 z, 2020.

677 Lohila, A., Aalto, T., Aurela, M., Hatakka, J., Tuovinen, J-P., Kilkki, J., Penttilä, T., Vuorenmaa, J.,
678 Hänninen, P., Sutinen, R., Viisanen, Y., and Laurila, T.: Large contribution of boreal
679 upland forest soils to a catchment-scale CH₄ balance in a wet year. *Geophysical
680 Research Letters* 43, 2946–2953, doi.org/10.1002/2016GL067718, 2016.

681 Marushchak, M.E., Kiepe, I., Biasi, C., Elsakov, V., Friborg, T., Johansson, T., Soegaard, H.,
682 Virtanen, T., and Martikainen, P.J.: Carbon dioxide balance of subarctic tundra from
683 plot to regional scales. *Biogeosciences* 10, 437–452, doi:10.5194/bg-10-437-2013,
684 2013.

Formatted: Subscript

685 McCalley, C.K., Woodcroft, B.J., Hodgkins, S.B., Wehr, R.A., Kim, E-H., Mondav, R., Crill, P.M.,
686 Chanton, J.P., Rich, V.I., Tyson, G.W., and Saleska, S.R.: Methane dynamics
687 regulated by microbial community response to permafrost thaw. *Nature* 514, 478–451,
688 doi:10.1038/nature13798, 2014.

689 McFadden, J.P., Eugster, W., and Chapin, F.S., III: A regional study of the controls on water vapor
690 and CO₂ exchange in arctic tundra. *Ecology* 84, 2762–2776, doi:10.1890/01-0444,
691 2003.

692 McGuire, A. D., Christensen, T. R., Hayes, D., Heroult, A., Euskirchen, E., Kimball, J. S., Koven,
693 C., Laflour, P., Miller, P. A., Oechel, W., Peylin, P., Williams, M., and Yi, Y.: An
694 assessment of the carbon balance of Arctic tundra: comparisons among observations,
695 process models, and atmospheric inversions, *Biogeosciences*, 9, 3185–3204,
696 <https://doi.org/10.5194/bg-9-3185-2012>, 2012.

697 McGuire, A.D., Lawrence, D.M., Koven, C., Clein, J.C., Burke, E., Chen, G., Jafarov, E.,
698 MacDougall, A.H., Marchenko, S., Nicolsky, D., Peng, S., Rinke, A., Ciais, P.,
699 Gouttevin, I., Hayes, D.J., Jin, D., Krinner, G., Moore, J.C., Romanovsky, V.,
700 Schädel, C., Schaefer, K., Schuur, E.A.G., and Zhuang, Q.: Dependence of the
701 evolution of carbon dynamics in the northern permafrost region on the trajectory of
702 climate change, *PNAS* 115.: 3882–3887, doi/10.1073/pnas.1719903115, 2018.

703 Mikola, J., Virtanen, T., Linkosalmi, M., Vähä, E., Nyman, J., Postanogova, O., Räsänen, A.,
704 Kotze, D.J., Laurila, T., Juutinen, S., Kondratyev, V., and Aurela, M.: Spatial
705 variation and linkages of soil and vegetation in the Siberian Arctic tundra – coupling
706 field observations with remote sensing data. *Biogeosciences* 15, 2781–2801, 2018.

707 Oh, Y., Zhuang, Q., Liu, L., Welp, L.R., Lau, M.C.Y., Onstott, T.C., Medvigy, D., Bruhwiler, L.,
708 Dlugokencky, E.J., Hugelius, G., D’Imperio, L., and Elberling, B. Reduced net
709 methane emissions due to microbial methane oxidation in a warmer Arctic. *Nature*
710 *Climate Change* 10, 317–321, 2020.

Formatted: Subscript

711 St Pierre, K.A., Kortegaard Danielsen, B., Hermesdorf, L., D'Imperio, L., Lønsmann Iversen, L.,
712 Elberling, B.: Drivers of net methane uptake across Greenlandic dry heath tundra
713 landscapes. *Soil Biology and Biochemistry* 138: 107605,
714 doi.org/10.1016/j.soilbio.2019.107605, 2019.

715 Räsänen, A., Manninen, T., Korhonen, M., Lohila, A., and Virtanen, T.: Predicting catchment-
716 scale methane fluxes with multi-source remote sensing. *Landscape Ecology* 36, 1177–
717 1195. <https://doi.org/10.1007/s10980-021-01194-x>. 2021.

718 Richardson, A.D.: Tracking seasonal rhythms of plants in diverse ecosystems with digital camera
719 imagery. *New Phytologist* 222,1742–1750, doi: 10.1111/nph.15591, 2019.

720 Sá, M.M.F., Schaefer, C.E.G.R., Loureiro, D.C., Simas, F.N.B., Alves, B.J.R., de Sá Mendonça, E.,
721 Barretto de Figueiredo, E., La Scala, N., Panosso, A.R., Fluxes of CO₂, CH₄, and N₂O
722 in tundra-covered and Nothofagus forest soils in the Argentinian Patagonia, *Science of*
723 *The Total Environment*, 659, 401-409,
724 <https://doi.org/10.1016/j.scitotenv.2018.12.328>, 2019.

725 Saunio, M., Stavert, A.R., Poulter, B., Bousquet, P., Canadell, J.G., Jackson, R.B., Raymond, P.A.,
726 Dlugokencky, E.J., Houweling, S., Patra, P.K. and Ciais, P.: The global methane
727 budget 2000–2017. *Earth System Science Data*, 12, 1561-1623, 2020.

728 Shaver, G.R., Street, L.E., Rastetter, E.B., van Wijk, M.T., and Williams, M.: Functional
729 convergence in regulation of net CO₂ flux in heterogeneous tundra landscapes in
730 Alaska and Sweden. *Journal of Ecology* 95, 802–817, 2007.

731 Street, L.E., Shaver, G.R., Williams, M., and van Wijk, M.T.: What is the relationship between
732 changes in canopy leaf area and changes in photosynthetic CO₂ flux in arctic
733 ecosystems? *Journal of Ecology* 95, 139–150, 2007.

734 Ter Braak, C.J.F. and Šmilauer, P.: Canoco reference manual and user's guide: software for
735 ordination (version 5.0). Microcomputer Power, Ithaca, NY, USA, 2012.

Formatted: Subscript

Formatted: Subscript

Formatted: Subscript

Formatted: Subscript

736 Treat, C.C., Marushchak, M.E., Voigt, C., Zhang, Y., Tan, Z., Zhuang, Q., Virtanen, T.A., Räsänen,
737 A., Biasi, C., Hugelius, G., Kaverin, D., Miller, P.A., Stendel, M., Romanovsky, V.,
738 Rivkin, F., Martikainen, P.J., and Shurpali, N.J. Tundra landscape heterogeneity, not
739 interannual variability, controls the decadal regional carbon balance in the Western
740 Russian Arctic. *Global Change Biology* 24, 5188–5204, doi: 10.1111/gcb.14421,
741 2018.

742 Tuovinen, J-P., Aurela, M., Hatakka, J., Räsänen, A., Virtanen, T., Mikola, J., Ivakhov, V.,
743 Kondratyev, V., and Laurila, T.: Interpreting eddy covariance data from
744 heterogeneous Siberian tundra: land-cover-specific methane fluxes and spatial
745 representativeness. *Biogeosciences* 16, 255–274, doi.org/10.5194/bg-16-255-2019,
746 2019.

747 Uttal, T., Starkweather, S., Drummond, J. R., Vihma, T., Makshtas, A. P., Darby, L. S., Burkhart,
748 J. F., Cox, C. J., Schmeisser, L. N., Haiden, T., Maturilli, M., Shupe, M. D., de Boer,
749 G., Saha, A., Grachev, A. A., Crepinsek, S. M., Bruhwiler, L., Goodison, B.,
750 McArthur, B., Walden, V. P., Dlugokencky, E. J., Persson, P. O. G., Lesins, G.,
751 Laurila, T., Ogren, J. A., Stone, R., Long, C. N., Sharma, S., Massling, A., Turner,
752 D. D., Stanitski, D. M., Asmi, E., Aurela, M., Skov, H., Eleftheriadis, K., Virkkula,
753 A., Platt, A., Førland, E. J., Iijima, Y., Nielsen, I. E., Bergin, M. H., Candlish, L.,
754 Zimov, N. S., Zimov, S. A., O'Neill, N. T., Fogal, P. F., Kivi, R., Konopleva-Akish,
755 E. A., Verlinde, J., Kustov, V.Y., Vassel, B., Ivakhov, V.M., Viisanen, Y., and Intrieri,
756 J. M.: International Arctic Systems for Observing the Atmosphere: An International
757 Polar Year Legacy Consortium. *Bull. Am. Meteor. Soc.*, 97, 1033–
758 1056. doi:10.1175/BAMS-D-14-00145.1, 2016.

759 Webb, E.E., Schuur, E.A.G., Natali, S.M., Oken, K.L., Bracho, R., Krapek, J.P., Risk, D., and
760 Nickerson, N.R.: Increased wintertime CO₂ loss as a result of sustained tundra

Formatted: Subscript

761 warming, *Journal of Geophysical Research Biogeosciences* 121, 249–265,
762 doi:10.1002/2014JG002795, 2016.

763 Wickland, K.P., Jorgenson, M.T., Koch, J.C., Kanevskiy, M., and Striegl, R.G.: Carbon dioxide and
764 methane flux in a dynamic Arctic tundra landscape: Decadal-scale impacts of ice
765 wedge degradation and stabilization. *Geophysical Research Letters*, 47,
766 e2020GL089894, doi:10.1029/2020GL089894, 2020.

767 van der Molen, M.K., van Huissteden, J., Parmentier, F.J.W., Petrescu, A.M.R., Dolman, A.J.,
768 Maximov, T.C., Kononov, A.V., Karsanaev, S.V., and Suzdalov, D.A.: The growing
769 season greenhouse gas balance of a continental tundra site in the Indigirka lowlands,
770 NE Siberia. *Biogeosciences* 4, 985–1003, doi.org/10.5194/bg-4-985-2007, 2007.

771 Virkkala, A.-M., Virtanen, T., Lehtonen, A., Rinne, J., and Luoto, M.: The current state of CO₂ flux
772 chamber studies in the Arctic tundra: A review. *Progress in Physical Geography*, 42,
773 162–184, 2018.

774 Virkkala, et al.: Statistical upscaling of ecosystem CO₂ fluxes across the terrestrial tundra and boreal
775 domain: regional patterns and uncertainties. *Global Change Biology*,
776 doi:10.1111/GCB.15659, 2021.

777 Virtanen, T. and Ek, M.: The fragmented nature of tundra landscape. *International Journal of*
778 *Applied Earth Observation and Geoinformation* 27, 4–12, 2014.

779 Zhang, W., Jansson, P-E., Sigsgaard, C., McConnell, A., Manon Jammot, M., Westergaard-Nielsen,
780 A., Lund, M., Friborg, T., Michelsen, A., and Elberling, B.: Model-data fusion to
781 assess year-round CO₂ fluxes for an arctic heath ecosystem in West Greenland (69°N).
782 *Agricultural and Forest Meteorology* 272–273, 176–186, 2019.

Formatted: Subscript

Formatted: Subscript

788
789
790
791
792
793
794
795
796
797
798
799
800
801
802
803

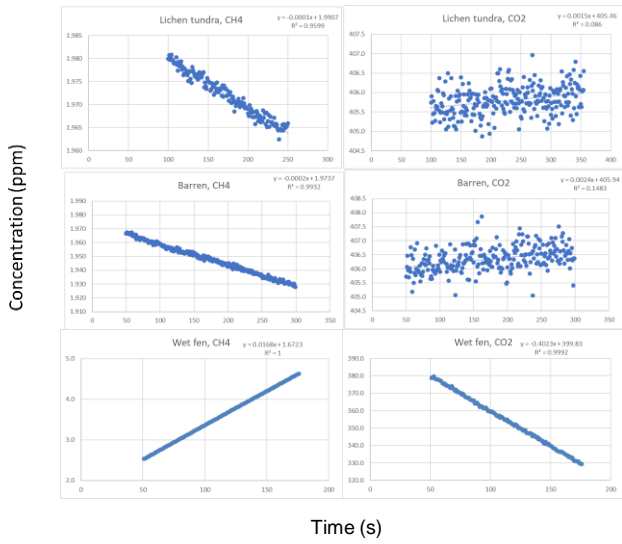
Appendix A



804
805
806
807
808
38

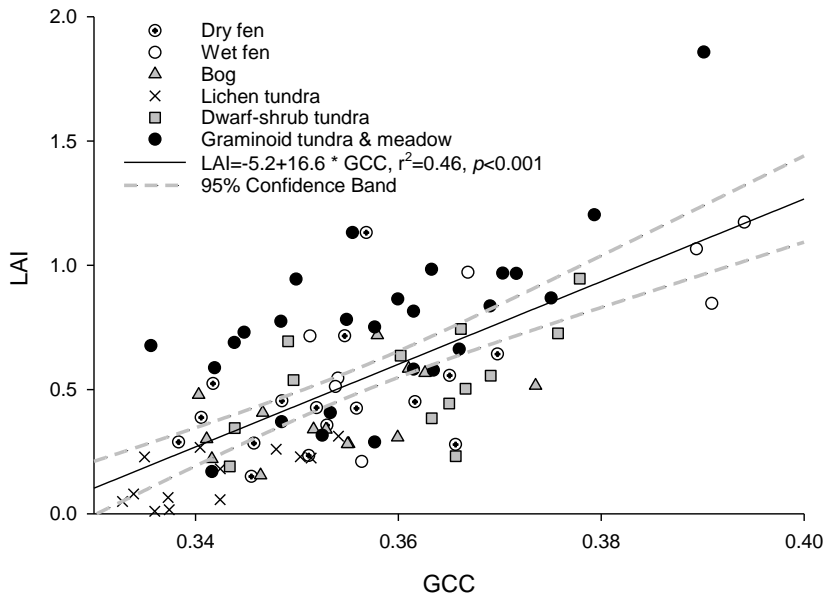
Fig. A1. Examples of the barren (left) and lichen tundra (right) plots with close views (bottom).
Vegetation consists of lichens *Flavocetraria* sp., *Thamnolia* sp., *Alectoria* sp., dwarf-shrubs *Dryas octopetala*, *Vaccinium vitis-idaea*, *Cassiope tetragona*, and graminoids and forbs such as *Carex* spp. and *Polygonum viviparum*.

809
810
811



812
813
814
815
816
817

Fig. A2. Examples of gas concentration variations during chamber closures measured using the gasRRG analyzer (DLT-100, Los Gatos Research, Inc., San Jose, CA, USA). The examples represent lichen tundra, barren, and wet fen.



818

819 Fig. A3. Relationship between GCC and vascular plant LAI in the harvested plots. LCTs are
 820 indicated with symbols. In the LCT-specific regressions (not shown), the coefficient of
 821 determination ($R^2_{adj.}$) was lowest for dry fen (0.06) and highest for wet fen (0.54). Regression
 822 slopes varied from 8.3 for dry fen to 17.8 for the combined graminoid tundra and meadow LCT.

823